Brain, Behavior, and Immunity 130 (2025) 106105

Contents lists available at ScienceDirect

Brain Behavior and Immunity

journal homepage: www.elsevier.com/locate/ybrbi

Full-length Article

CD300f enables microglial damage sensing, efferocytosis, and apoptotic cell metabolization after brain injury

Luciana Negro-Demontel [a,b,c,*], Frances Evans [a,b], Fabio Andrés Cawen [b,d,e], Zachary Fitzpatrick [c], Hannah D. Mason [c], Daniela Alí-Ruiz [b], Rubèn López-Vales [f,g,h], Natalia Lago [f,g,h], Hugo Peluffo [b,d,e,**]

[a] Department of Histology and Embriology, School of Medicine, UDELAR, Montevideo, 11800, Uruguay
[b] Institut Pasteur de Montevideo, Montevideo, 11400, Uruguay
[c] National Institute of Neurological Disorders and Stroke (NINDS), National Institutes of Health (NIH), Bethesda, MD, USA
[d] Unitat de Bioquímica i Biologia Molecular, Departament de Biomedicina, Facultat de Medicina i Ciències de la Salut, Universitat de Barcelona (UB), 08036, Spain
[e] Institut de Neurociències, Universitat de Barcelona (UB), 08036, Spain
[f] Departament de Biologia Cel·lular, Fisiologia i Immunologia, Universitat Autònoma de Barcelona (UAB), Spain
[g] Institut de Neurociències, Autonomous University of Barcelona (UAB), Spain
[h] Centro de Investigación Biomédica en Red sobre Enfermedades Neurodegenerativas (CIBERNED), Spain

ARTICLE INFO

Keywords:
Microglia
Efferocytosis
CD300f
CD300lf
DAMP
TBI
Phagocytosis
Neuroinflammation

ABSTRACT

Microglia, the resident phagocytes of the central nervous system (CNS), continuously survey the parenchyma and its borders, acting as first responders to brain injury. Their ability to detect and react to environmental changes is mediated by a repertoire of surface receptors collectively known as the microglial sensome.

Here, we identify the lipid-sensing immunoreceptor CD300f as a key regulator of microglial responses to tissue damage and apoptotic cells. Using intravital two-photon microscopy, we show that CD300f$^{-/-}$ microglia fail to extend processes toward a laser-induced cortical lesion, indicating impaired detection of damage-associated cues.

In models of mild traumatic brain injury (mTBI) and intracortical injection of apoptotic cells, CD300f deficiency led to reduced recognition and clearance of dying cells resulting in the accumulation of cellular debris within the parenchyma. At later stages, apoptotic remnants were retained within CD300f$^{-/-}$ microglia *in vivo* and bone marrow–derived macrophages *in vitro*, suggesting defective intracellular degradation.

Proteomic analysis after a controlled cortical injury (CCI) contusion model revealed widespread dysregulation of autophagy-related and metabolic pathways, consistent with impaired efferocytosis and phagolysosomal processing. In parallel, we observed upregulation of the UDP-degrading ectonucleotidase ENTPD6 protein and downregulation of the microglial purinergic receptor P2ry6 mRNA, indicating a dysfunctional UDP–P2RY6 axis that may underlie impaired damage sensing and phagocytic initiation.

Despite greater histological preservation, CD300f$^{-/-}$ mice exhibited worse long-term functional recovery after brain injury.

Together, these findings highlight CD300f as a key damage-associated molecular pattern (DAMP) receptor that integrates purinergic signaling, efferocytosis, and metabolic adaptation, highlighting its essential role in coordinating microglial responses to CNS injury.

1. Introduction

Microglia, the innate immune cells of the CNS, play essential roles in maintaining tissue homeostasis and responding to injury. Their ability to monitor the neural parenchyma (Davalos, 2005; Nimmerjahn et al., 2005) is mediated by a diverse repertoire of receptors, collectively referred to as the microglial sensome (Hickman, 2013). This receptor battery enables microglia to prune synapses, detect pathogens and

* Corresponding author at: Department of Neurology, Washington University School of Medicine, St Louis, Missouri 63110, USA.
** Corresponding author at: Unitat de Bioquímica i Biologia Molecular, Departament de Biomedicina, Facultat de Medicina i Ciències de la Salut, Universitat de Barcelona (UB), 08036, Spain.
E-mail addresses: Lucianan@wustl.edu (L. Negro-Demontel), hugo.peluffo@ub.edu (H. Peluffo).

https://doi.org/10.1016/j.bbi.2025.106105
Received 20 February 2025; Received in revised form 2 September 2025; Accepted 6 September 2025
Available online 9 September 2025
0889-1591/© 2025 The Author(s). Published by Elsevier Inc. This is an open access article under the CC BY-NC license (http://creativecommons.org/licenses/by-nc/4.0/).

damage-associated molecular patterns (PAMPs and DAMPs) and clear apoptotic cells, myelin debris, and toxic lipids and proteins like Aβ (De Schepper et al., 2021).

Following CNS injury, substantial amounts of DAMPs—including purines and lipid mediators—are released into the extracellular space, shaping the activation and phenotypic transformation of microglia. Lipid molecules such as phosphatidylserine (PS), oxidized phospholipids, and lipoproteins are key modulators of microglial phagocytic and inflammatory responses. These signals are recognized in part via TAM receptors (Fourgeaud, 2016) (e.g., Mertk, Axl) and TREM2, which regulate microglial efferocytosis and sensing of tissue damage (Cignarella, 2020; Takahashi et al., 2005; Mazaheri, 2017). In parallel, extracellular purines such as ATP and UDP engage purinergic receptors—including P2Y6, P2Y12, and P2X7—to regulate microglial chemotaxis, cytokine production, and efferocytosis (Davalos, 2005; Koizumi, 2007; Nimmerjahn et al., 2005). Together, these metabolites contribute to the dynamic remodeling of microglial states after injury. While several receptors have been implicated in sensing these cues, the mechanisms by which microglia coordinate responses to complex DAMP landscapes remain incompletely understood.

Recent transcriptomic analyses identified the lipid-sensing immune receptor CD300f as part of a core injury-activated microglia/macrophage (IAM) gene signature following spinal cord injury (Wahane, 2021). However, whether CD300f plays a role in microglial responses to acute CNS injury, including efferocytosis and metabolic adaptation, remains unknown. CD300f, which shares several ligands and downstream signaling pathways with TREM2. It specifically binds PS and other endogenous lipids and lipoproteins, facilitating the recognition and engulfment of apoptotic cells by macrophages *in vitro* (Tian, 2014; Choi, 2011). CD300f is a unique myeloid receptor capable of delivering both activating and inhibitory signals (Alvarez-Errico et al., 2007; Alvarez-Errico, 2004), in part through its physical interaction with IL4Rα which is required for robust IL-4 responses (Moshkovits, 2015). Sensing of apoptotic cells, combined with IL-4 signaling, launches an anti-inflammatory and tissue repair response in macrophages in a wide range of biological contexts (Bosurgi,)implicating a role for CD300f. CD300f deficiency has been linked to worsened outcomes in models of experimental autoimmune encephalomyelitis (EAE) and increased risk in systemic lupus erythematosus (SLE) (Xi, 2010).

In the brain, CD300f is uniquely expressed by microglia and barrier macrophages (Lago, 2020). Previous studies from our group have shown that CD300f regulates microglial metabolic fitness in models of aging (Frances Evans, 2023) and neuropsychiatric disease (Lago, 2020). Its deletion reduces expression of the phagocytic marker SPP1 and is associated with cognitive (Frances Evans, 2023) and behavioral impairments, including features relevant to depressive- and anxiety-like phenotypes (Lago, 2020; Kaufmann, 2021), as well as altered microglia-mediated synaptic pruning *in vitro* (Lago, 2020). Endogenous CD300f contributes to neuronal viability following penetrating brain injury, while its overexpression is neuroprotective in acute brain injury (Peluffo, 2012), and associated with improved neurological performance in Tau and Aβ Alzheimer's disease models (McManus, 2022; Ising, 2019). Together, these findings position CD300f as a critical regulator of microglial homeostatic and phagocytic functions.

Here, we hypothesize that CD300f functions as a key injury-sensing receptor that enables microglia to rapidly detect, engulf, and degrade apoptotic cells following CNS trauma. Using *in vivo* imaging and mouse models of mild and contusive traumatic brain injury (CCI), we show that CD300f is required for microglial process extension toward injured tissue, efficient efferocytosis and apoptotic cell degradation, and functional recovery (Fig. 1a). In the absence of CD300f, P2RY6 expression fails to increase after CCI, suggesting impaired purinergic signaling. To gain mechanistic insight, we performed quantitative proteomics 24 h post-CCI injury, which revealed a significant upregulation of ENTPD6, an ectonucleoside triphosphate diphosphohydrolase (CD39L2) that degrades extracellular UDP to UMP (Ivanenkov et al., 2003; Hicks-Berger et al., 2000). In addition, we observed widespread alterations in autophagic, mitophagic, and metabolic pathways.

Collectively, our results identify CD300f as a critical component of the microglial sensome, orchestrating the detection of tissue damage, clearance of apoptotic cells, and downstream metabolic adaptation following CNS injury (see Fig. S1 for a graphical summary of the proposed mechanism).

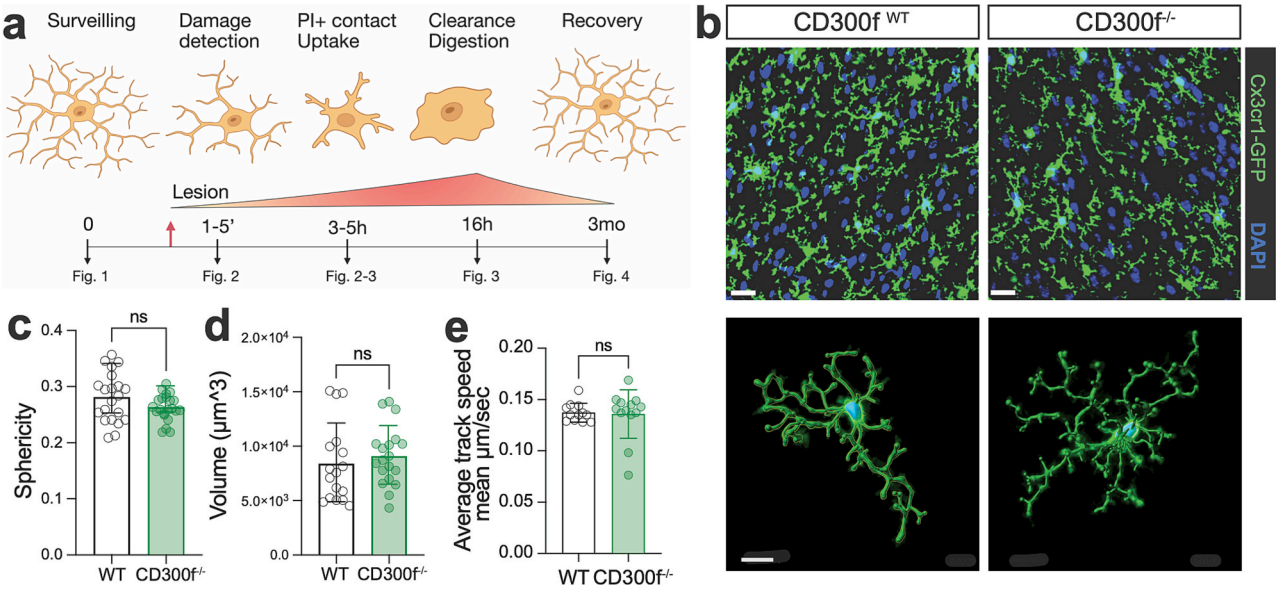

Fig. 1. CD300f deficiency does not affect microglial morphology or dynamics at rest. a) Schematic overview of the experimental timeline and microglial states following cortical injury, b) Representative confocal images of the cortex from naïve CX3CR1$^{+/GFP}$ CD300f$^{-/-}$ and WT showing homeostatic microglia (green CX3CR1-GFP, blue DAPI). Bottom: reconstructions of microglia captured by intravital two-photon microscopy. c-d) Quantification of microglial sphericity (c) and volume (d) n = 3 mice per group, 5 images per mouse. e) Average track speed of surveilling microglial processes. n = 6 mice per group, 12 cells per genotype. Error bars: mean ± SEM. ns = not significant. (For interpretation of the references to colour in this figure legend, the reader is referred to the web version of this article.)

2. Results

2.1. CD300f deficiency does not alter baseline microglial morphology or dynamics

To test whether CD300f regulates acute microglial responses, we generated CX3CR1$^{+/GFP}$/CD300f$^{-/-}$ mice and applied complementary models of acute brain injury to assess microglial responses *in vivo*. The schematic timeline in Fig. 1a illustrates the progression of microglial states following injury—from baseline surveillance through damage detection, efferocytosis, and recovery. CD300f deficiency did not significantly alter homeostatic microglial morphology (Fig. 1b-d) or baseline process motility (Fig. 1e; Movie 1).

2.2. CD300f is required for microglial process recruitment and morphological transformation after injury

To induce localized release of DAMPs we performed focal laser

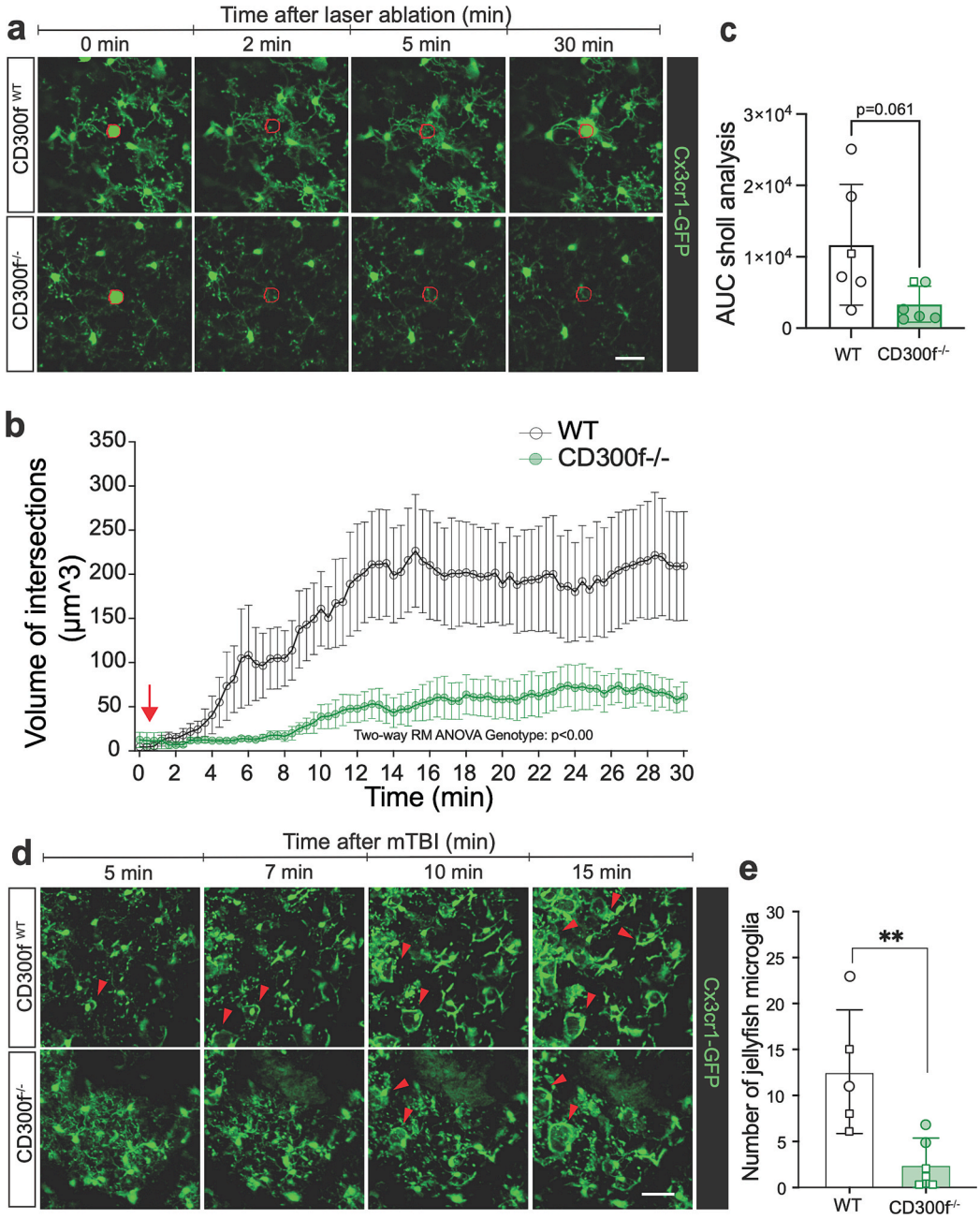

Fig. 2. CD300f contributes to the microglial damage sensing response. a) Representative intravital two-photon microscopy stills showing WT and CD300f$^{-/-}$ acute microglial responses (CX3CR1-GFP, green) to focal laser ablation through a thinned-skull window. Red circles indicate ablation sites. Scale bar: 20 µm. b–c) Quantification of microglial process recruitment toward the lesion using volumetric Scholl analysis. b) Time course of projection volume; red arrow marks time of ablation (Two-way ANOVA, genotype $p = 0.043$; time, time x genotype and subject all $p < 0.0001$). c) Area under the curve (AUC) analysis for projection volume from b (two-tailed Student's *t*-test with Welch's correction *$p < 0.05$). n = 6 mice per genotype (1 female (square); 5 male). Total number of lesions = 10 wt; 12 CD300f$^{-/-}$. d) Two-photon time-lapse stills showing jellyfish-like phagocytic microglia morphological transformation in WT and CD300f−/− brains, minutes after mTBI. Arrowheads indicate jellyfish microglia. Scale bar: 40 µm. e) Quantification of jellyfish-like microglia. Student's *t*-test. $p < 0.01$ (F test $p = 0.091$). n = 5 wt (3 female (squares); 2 male), 6 CD300f$^{-/-}$ (3 female (squares); 3 male). (For interpretation of the references to colour in this figure legend, the reader is referred to the web version of this article.)

ablations in the cortex and monitored the immediate microglial response using intravital two-photon microscopy. In the absence of CD300f, we observed a significant reduction in microglial projection recruitment - toward the lesion site (Fig. 2a-c; Movie 2), despite some inter-animal variability (Fig. S2a–b).

We next tested whether CD300f contributes to microglial sensing of tissue damage and apoptotic cells, we employed a mild cortical traumatic brain injury (mTBI) model (Roth, 2014). This paradigm elicits the release of apoptotic cells, debris, reactive oxygen species (ROS), and purinergic DAMPs, notably UDP, which has been shown to drive microglial transformation into the phagocytic "jellyfish" phenotype via P2RY6 signaling (Roth, 2014). Under these conditions, we observed a significant reduction in phagocytic, jellyfish-like microglia in CD300f-deficient lesions by intravital two-photon imaging (Fig. 2d, e; Movie 3).

Together, these results indicate that CD300f is required for efficient microglial recruitment and morphological transformation in response to acute cortical damage. Although CD300f$^{-/-}$ microglia are appropriately positioned near dying cells, their reduced process extension and morphological activation suggest a diminished capacity to interpret local damage-associated cues. These defects may hinder downstream

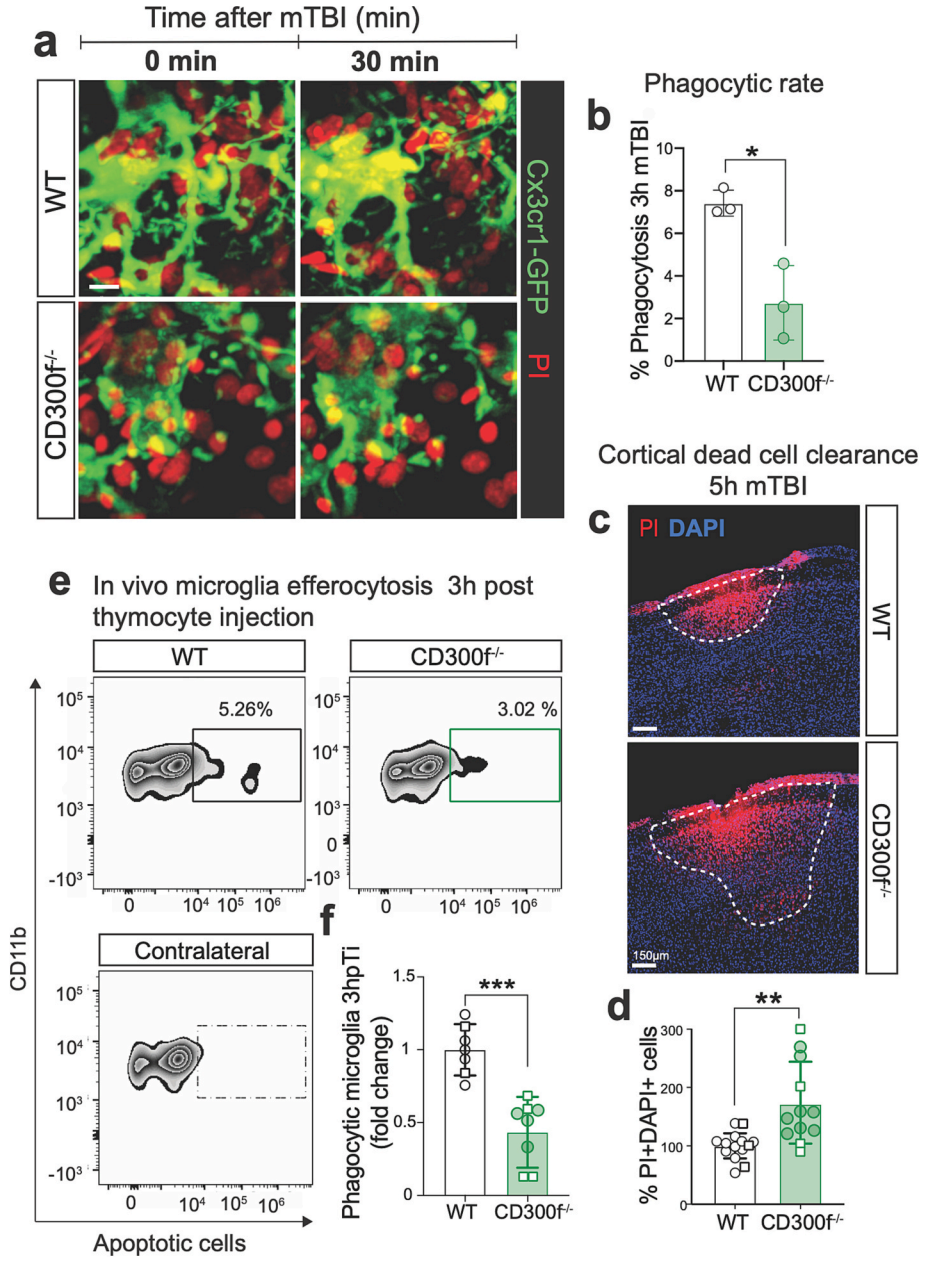

Fig. 3. CD300f is required for microglial detection, engulfment, and degradation of dead/apoptotic cells. a) Representative intravital two-photon microscopy stills showing CX3CR1^{+}/GFP microglia (green) engulfing PI^{+} dead cells (red) 3 h post-mTBI in WT and CD300f$^{-/-}$ mice. Scale bar: 10 µm. b) Quantification of the microglial phagocytic index over a 30-minute time window. Data represent mean ± SEM from 3 independent experiments (1 male mouse/genotype per experiment). Two-tailed Student's *t*-test. *p < 0.05 (F test p = 0.217). c) Representative confocal images from cortical sections 5 h after mTBI showing dying cells (PI^{+}, red), and nuclei (DAPI, blue). bars: 150 µm. d) Quantification of PI^{+} cell accumulation in the lesion core. WT n = 14 (3 female (squares); 11 male,); CD300f$^{-/-}$: KO n = 12 (4 female, 8 male). Two-tailed Student's *t*-test. **p < 0.01. e) Flow cytometry plots showing uptake of fluorescently labeled apoptotic thymocytes (ATs) by microglia 3 h post-injection into the cortex. f) Quantification of AT uptake as fold change over contralateral hemisphere. Data from 4 independent experiments. WT n = 7 (3 female (squares); 4 male); KO n = 8 (4 female 4 male). Student's *t*-test. ***p < 0.001. (For interpretation of the references to colour in this figure legend, the reader is referred to the web version of this article.)

efferocytic functions, prompting us to investigate apoptotic cell recognition and clearance in more detail.

2.3. CD300f-Deficient microglia show impaired apoptotic cell clearance and degradation

To assess whether microglial CD300f contributes to the *in vivo* efferocytosis of apoptotic cells, we labeled acutely injured cells with propidium iodide (PI) via transcranial and i.p. application and quantified the frequency of PI^+ cells engulfed by CX3CR1-GFP^+ microglia after mTBI using two-photon microscopy. At 3 h post-injury, $CD300f^{-/-}$ microglia exhibited a significantly reduced phagocytic index compared to WT (Fig. 3a, b; Movie 4). Supporting this observation, histological analysis of brain sections stained with DAPI and PI 5 h post-mTBI revealed increased retention of PI^+ cells in the lesion core of CD300f-deficient mice (Fig. 3c–d), as well as in the perilesional area (Fig. S2c, d, g). We measured the distance between PI^+ cells and $Iba1^+$ microglia in the perilesional cortex. Although the average shortest distance per animal was not significantly different (Fig. S2e), there was a trend toward increased spacing. Notably, when analyzed per cell, the distribution of shortest distances was significantly higher in $CD300f^{-/-}$ mice, indicating impaired microglial contact with apoptotic targets (Fig. S2f–g). These data support the notion that CD300f deficiency reduces the efficiency of apoptotic cell engagement and clearance *in vivo*. To directly test microglial efferocytic function *in vivo*, we injected fluorescently labeled apoptotic thymocytes (ATs) into the cortex of WT and $CD300f^{-/-}$ mice and assessed uptake 3 h later by flow cytometry (Fig. 3e–f; Movie 5). $CD300f^{-/-}$ microglia showed significantly impaired AT uptake, confirming defective recognition and engulfment of apoptotic targets.

Given these early defects, we next investigated whether CD300f also regulates the degradation of internalized cargo, as previously shown for TREM2-deficient microglia (Nugent, 2020). To this end, we performed a pulse-chase assay using bone marrow-derived macrophages (BMDMs) from WT and $CD300f^{-/-}$ mice (Fig. 4a). After a 15-minute pulse with ATs, $CD300f^{-/-}$ BMDMs demonstrated reduced engulfment (Fig. 4b, left). Strikingly, after a 4-hour pulse followed by a 16-hour chase, CD300f-deficient cells retained significantly more AT-derived signal WT, suggesting impaired degradation of engulfed apoptotic cells (Fig. 4b, right). Consistent with these findings, flow cytometric analysis of microglia 16 h after mTBI revealed elevated retention of PI^+ debris in $CD300f^{-/-}$ cells compared to WT (Fig. 4c). Together, these results

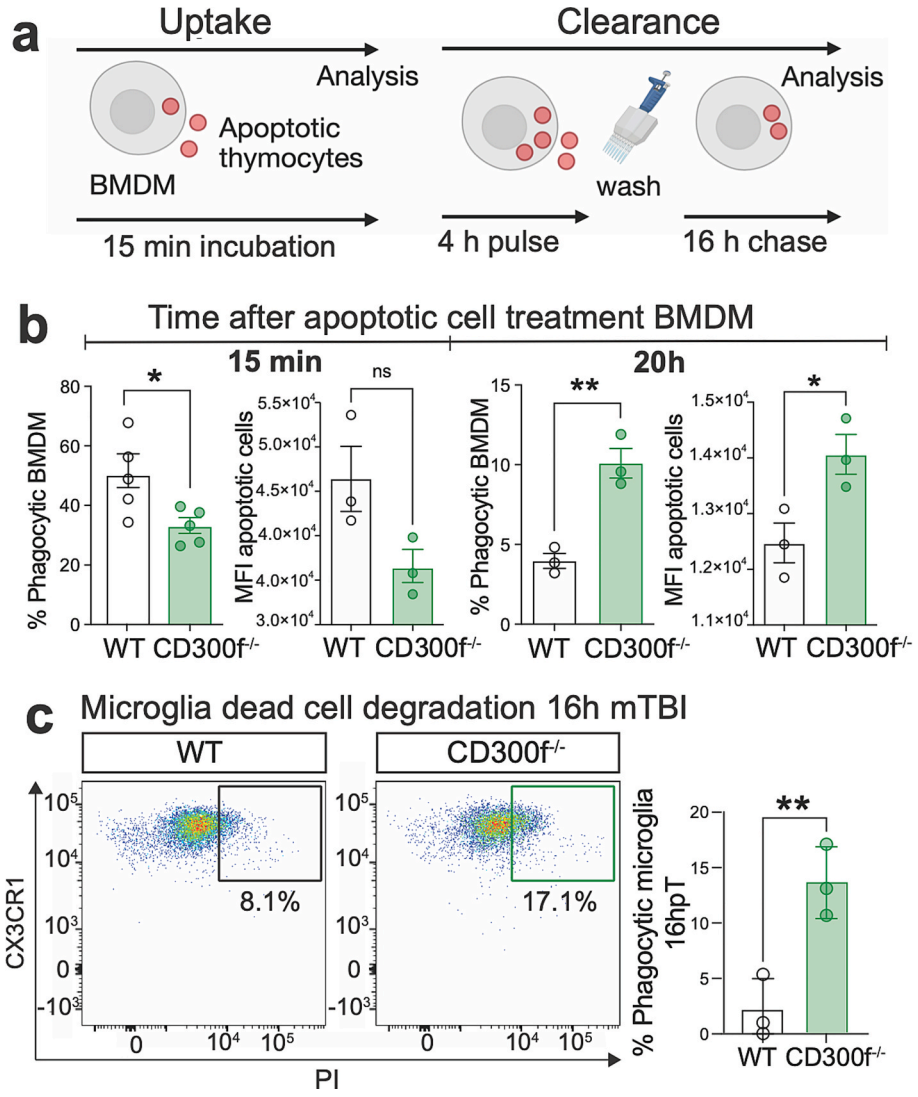

Fig. 4. Microglia use CD300f to degrade engulfed cells. a) Schematic of pulse-chase assay using BMDMs exposed to ATs for either 15 min or 4 h (pulse), followed by a 16 h chase. b) Left: % of phagocytic BMDMs 15 min post-AT exposure. Right: Retained AT signal (gMFI) 20 h post-pulse. Data from 3 independent experiments (n = 3 mice/group). Student's *t*-test. *$p < 0.05$, **$p < 0.01$. c) Flow cytometry plots and quantification of PI^+ debris-retaining microglia 16 h after mTBI. Data pooled from 3 independent experiments (3–5 mice/group per experiment). Student's *t*-test. **$p < 0.01$.

demonstrate that CD300f is required for both efficient apoptotic cell clearance and subsequent degradation of phagocytosed material by microglia.

2.4. CD300f deficiency selectively impairs neutrophil recruitment without disrupting barrier integrity

To exclude the possibility that impaired microglial efferocytosis in CD300f$^{-/-}$ mice arises from differences in barrier integrity or peripheral immune infiltration, we evaluated glia limitans permeability and immune cell recruitment to the dura following mTBI (Roth, 2014; Nimmerjahn et al., 2004). Intravital two-photon microscopy following transcranial application of the low-molecular-weight dye SR101 revealed no genotype-dependent differences in dye diffusion across the glia limitans (Fig. 5a, b), indicating that barrier integrity is preserved in CD300f$^{-/-}$ mice post-mTBI.

Next, we evaluated leukocyte infiltration into the dura. Although the number of CD11b^{+} myeloid cells and the burden of PI^{+} cell death was comparable between genotypes (Fig. 5c-e), CD300f$^{-/-}$ mice exhibited a selective reduction in Ly6G^{+} neutrophil accumulation at the dura lesion 5 h post injury (Fig. 5f, g). This finding was confirmed by intravital two-photon microscopy (see Movie 6), which showed a robust influx of Gr1^{+} cells into WT dura, markedly reduced in CD300f$^{-/-}$ mice. The reduction in neutrophil recruitment was accompanied by a trend toward lower expression of the neutrophil-attracting chemokine *Cxcl1* and *Ccl3* levels in CD300f$^{-/-}$ cortex (Fig. 5h, i), suggesting that resident myeloid cells fail to mount appropriate chemokine responses to injury cues in the absence of CD300f.

Finally, given prior reports linking myeloid cell activity to vascular remodeling after trauma (Russo et al., 2018), we assessed meningeal vascular repair at 7 days post-mTBI. Quantification of revascularization revealed no significant differences in vessel regrowth between genotypes (Fig. 5j, k), indicating that CD300f is dispensable for vascular recovery despite altered neutrophil responses.

Together, these findings suggest that CD300f deficiency does not disrupt barrier integrity or general leukocyte infiltration but specifically

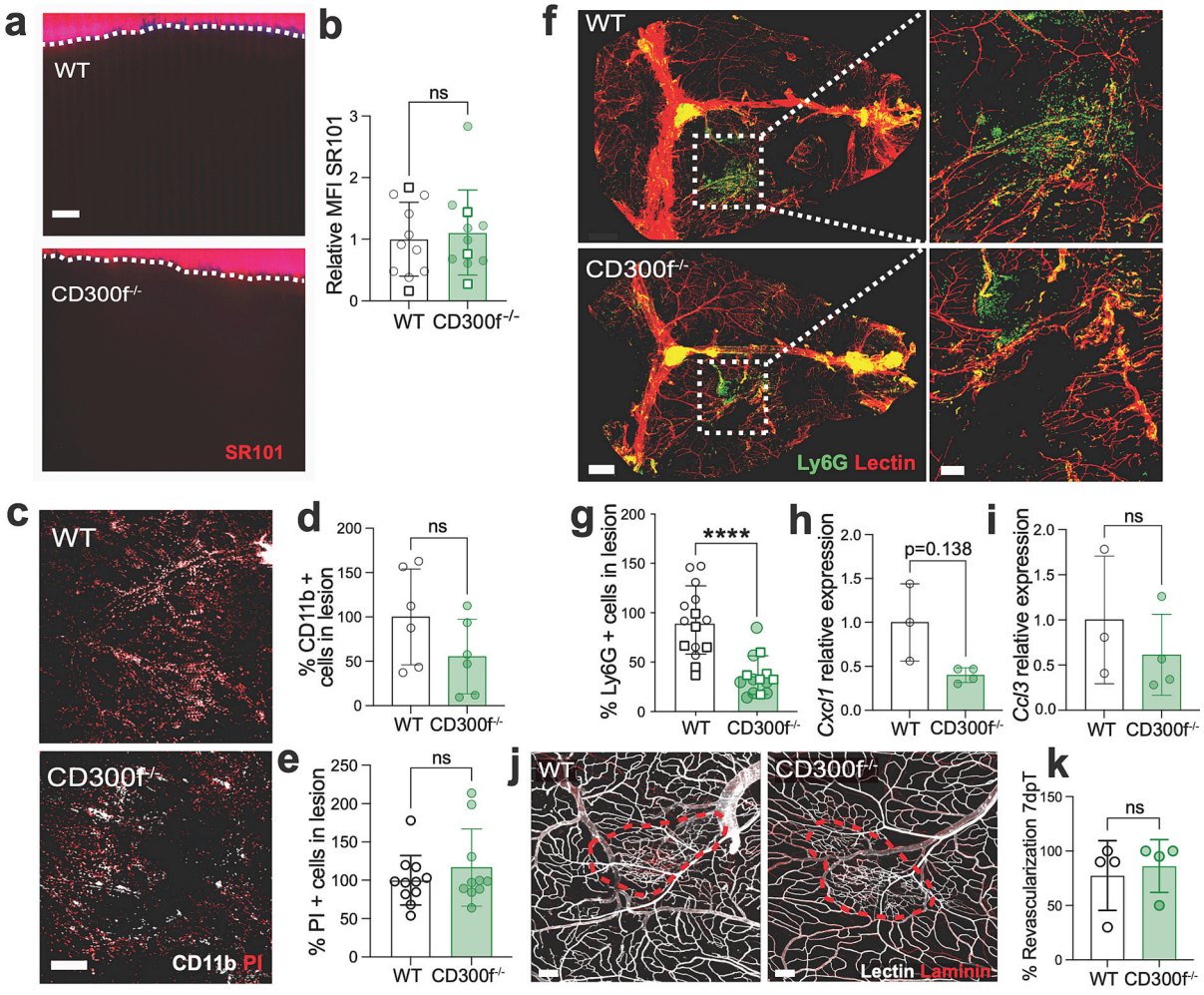

Fig. 5. CD300f deficiency does not compromise glial limitans integrity or global meningeal responses but impairs neutrophil recruitment to the dura following mTBI. a, b) SR101 assay. Data representative from 3 independent experiments. WT $n = 11$ (2 female (square); 9 male), KO n = 11 (3 female; 8 male). Scale bar 30 μm c-d) Monocyte counts in lesion; CD11b+ (white) PI+ (red) $n = 6$. e) Meningeal cell death quantification PI + cells in lesion. $n = 11$ (WT), 10 (KO). Scale bar 200 μm. Two-tailed Student's *t*-test, ****p < 0.0001. Confocal images of meningeal whole mounts stained for Ly6G (neutrophils, green) Lectin (blood vessels, red). f) Representative confocal stacks of whole mount meninges 5 h post-mTBI, stained with Ly6G (green) and lectin (blood vessels, red). g) Neutrophil recruitment to dura 5 h post-mTBI. Ly6G^{+} neutrophil counts within the lesion, expressed as relative frequency normalized to WT. Data pooled from 6 independent experiments. WT $n = 15$ (6 female (squares); 9 male), KO $n = 14$ (6 female; 8 males). Scale bar 1000 μm and 300 μm. h-i) Relative expression of *Cxcl1* and *Ccl3* mRNA in brain punctures 5 h after mTBI. $n = 3$ (WT), 4 (KO). j) Meningeal revascularization; Representative confocal images of meningeal whole mounts 7 days post-mTBI. Lesion (dotted red line), laminin (red), lectin (white). Scale bar 200 μm. n = 4 males. K) Quantification of meningeal revascularization index. Two-tailed Student's *t*-test with Welch's correction (F test p = 0.024) in h and two-tailed Student's *t*-test*p < 0.05 in all other graphs. (For interpretation of the references to colour in this figure legend, the reader is referred to the web version of this article.)

impairs neutrophil recruitment to the dura and local chemokine production following mTBI.

2.5. CD300f deficiency worsens long-term recovery despite reduced tissue loss after CCI

To investigate the long-term neurological consequences of CD300f deficiency, we employed a more severe model of focal brain trauma using controlled cortical impact (CCI). Motor coordination was assessed longitudinally using the parallel rod floor test, a validated assay for detecting both acute and chronic deficits following CCI (Richter, 2018). CD300f$^{-/-}$ mice displayed significantly impaired recovery of motor performance] compared to WT, with elevated error rates persisting throughout the 90-day post-injury period (Fig. 6a, Fig. S4a). Importantly, spontaneous locomotor activity remained similar across genotypes (Fig. S4b–c), ruling out general motor impairments as a confounding factor. Surprisingly, despite worse functional outcomes, CD300f$^{-/-}$ mice exhibited smaller lesion volumes at 90 days post-CCI, as shown by cresyl violet staining (Fig. 6b-d). Quantification revealed reduced cortical area and volume loss in CD300f$^{-/-}$ brains. This was paralleled by increased NeuN^{+} neuronal density in the perilesional cortex of CD300f$^{-/-}$ animals (Fig. 6e, f).

To examine microglial activation states, we performed morphometric analysis of Iba1^{+} microglia in the perilesional cortex as previously described (Henry, 2019). CD300f$^{-/-}$ brains exhibited shift away from amoeboid, phagocytic morphology toward more ramified, primed phenotypes (Fig. 6g, h). consistent with deficient DAMP sensing and efferocytosis observed in earlier experiments.

These data suggest that loss of CD300f uncouples structural preservation from functional recovery, likely due to insufficient microglial activation and failure to clear apoptotic debris effectively.

2.6. CD300f regulates expression of efferocytic genes and metabolic remodeling after brain injury

To further explore the molecular mechanisms underlying impaired microglial function in CD300f$^{-/-}$ mice, we assessed the expression of genes associated with phagocytosis and acute inflammation in brain tissue 1-day post-CCI (Fig. 7a, S4d, e). CD300f deficiency led to a blunted upregulation of *P2ry6* mRNA, a purinergic receptor that mediates microglial chemotaxis and phagocytosis in response to DAMPs. Additionally, the expression of two other microglial receptors critical for phagocytosis—*Sirpβ1a* (Gaikwad, 2009) and *F2rl1* (Jaffa, 2021)—was significantly downregulated in CD300f$^{-/-}$ brains, suggesting a broad impairment in phagocytic programming.

Notably, the expression of classical pro-inflammatory cytokines

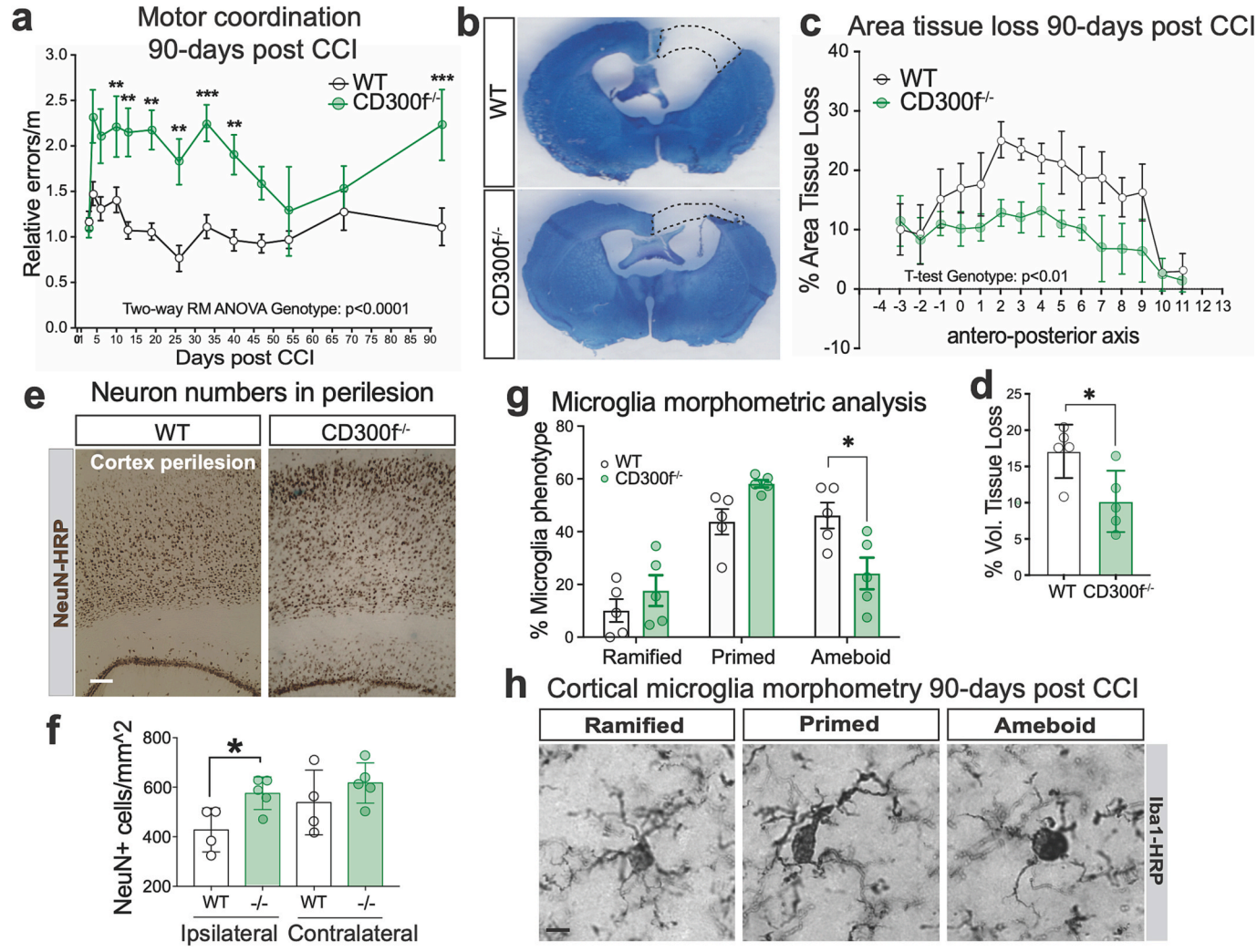

Fig. 6. CD300f deficiency leads to dysregulation of purinergic signaling, efferocytosis and metabolic pathways after CCI. a) Relative mRNA expression of phagocytosis-related genes (*P2ry6, Sirpβ1a,* and *F2rl1*) in WT and CD300f−/− cortex at 1-day post-CCI. Two-tailed Student's *t*-test, *p < 0.05, **p < 0.01; *n* = 3–6 mice per group. b) Volcano plot representing the differentially expressed proteins obtained by DIA proteomics. c, d) Kegg protein pathway enrichment in the lesion, 1 day after CCI.

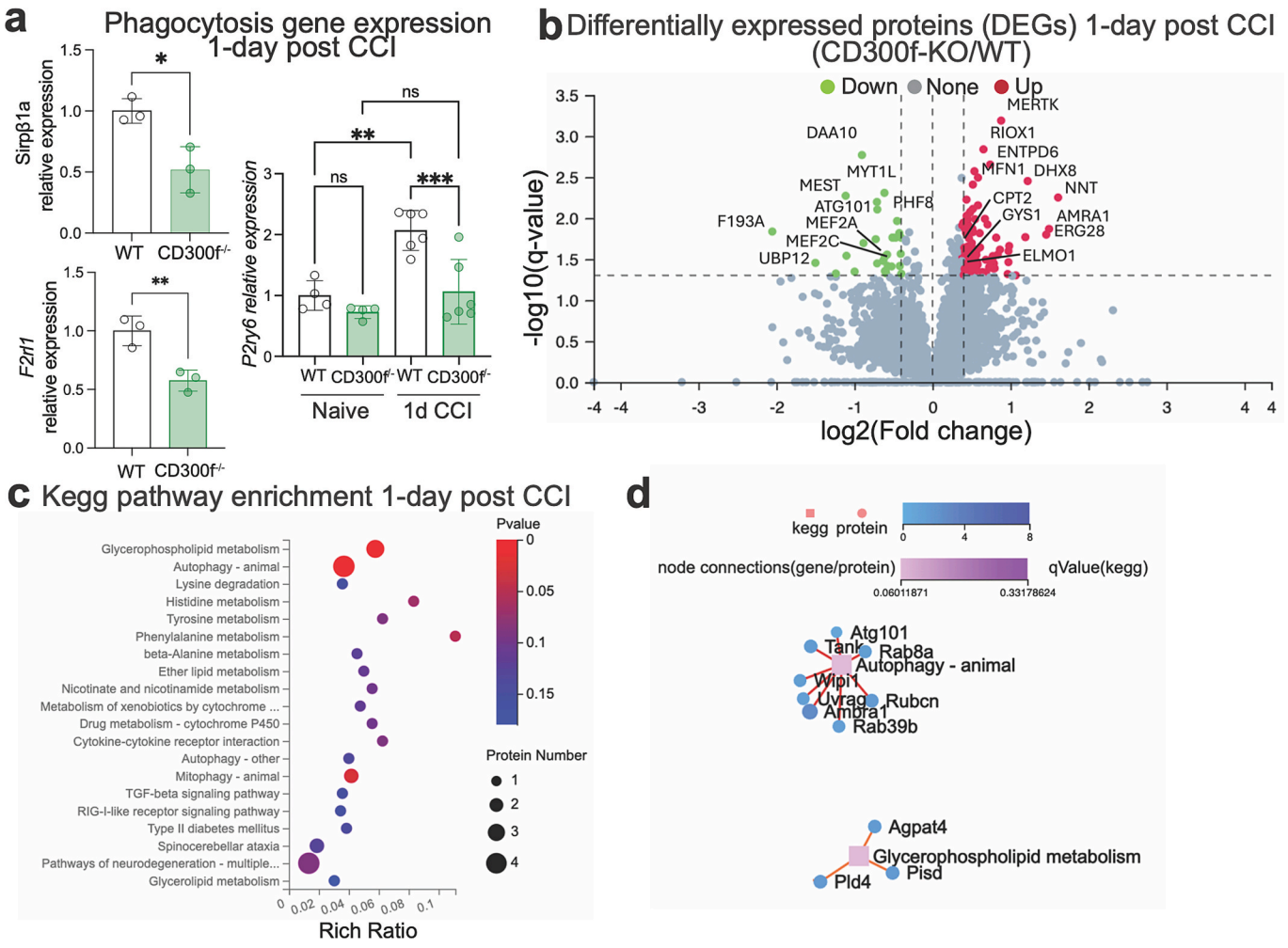

Fig. 7. CD300f is required for coordinated purinergic signalling, efferocytosis, and metabolic remodelling following CCI.

including *Il1β, Ifnγ, Tnfα,* and *Il6* remained unchanged (Fig. S4d, e), indicating that the observed functional and transcriptional changes are not due to heightened neuroinflammation.

To validate these transcriptional changes at the protein level, we performed quantitative proteomics on the lesion and perilesional cortex 1-day post-CCI. Across 7000 proteins identified per sample we detected 173 differentially expressed proteins ($p < 0.05$). In line with the transcript data, expression of major proinflammatory markers such as microglia/macrophage AIF1 (IBA1) or ITGAM (CD11b), astroglial GFAP, or general mediators such as NFKB1, NFKB2, IL33, IL16, IL18, NFKBIB (IKKB), STAT1, STAT2, STAT3, PTGS1 (COX1), PTGS2 (COX2), NOS1, MMP9, CTSB, CTSC, LAMP1, or CASP3 was unchanged. Similarly, canonical homeostatic microglial proteins—including TMEM119, P2RY12 and HEXB —remained stable.

In contrast, CD300f deficiency triggered broad dysregulation of cellular clearance and metabolic pathways. KEGG analysis showed significant enrichment in proteins involved in autophagy (ATG101, RUBCN, TANK, AMBRA1, TBC1D5, WIPI1, RAB8A, UVRAG), mitophagy (MFN1, WIPI1, USP30, AMBRA1) and glycerophospholipid metabolism (PISD, PLD4, AGPAT4). In. parallel, several key enzymes involved in lipid (LIPA, ABCD3, ACADVL, ACAD9, MLYCD, ACSBG1) and glycogen metabolism (GYS1, PHKA1 and PGM2) were upregulated. Strikingly, key components of the apoptotic cell clearance machinery—the efferocytic receptor MERTK (Scott, 2001) and the intracellular adaptor ELMO1, which coordinate engulfment and cytoskeletal remodeling during efferocytosis (Park, 2007)—were among the most upregulated proteins. Additionally, we detected significant increase in ENTPD6 (CD39L2), an ectonucleotidase that degrades extracellular UDP (Hicks-Berger et al., 2000) a primary ligand for P2RY6. This suggests that excessive UDP degradation may compromise damage sensing, potentially perpetuating the efferocytic dysfunction in CD300f$^{-/-}$ microglia.

In sum, CD300f deletion disrupts transcriptional and metabolic programs that enable microglia to recognize, engulf, and degrade apoptotic material after injury. These molecular defects may underlie the uncoupling of functional recovery from structural preservation observed in CD300f-deficient mice, highlighting the critical role of CD300f in coordinating appropriate microglial activation and phagocytosis in the aftermath of trauma.

3. Discussion

Understanding the microglial sensome and the signals that direct responses to tissue injury, apoptotic cells, or infection is essential, as they constitute critical triggers that drive the adoption of distinct microglial states, ultimately shaping pathological and functional outcomes. Gaining deeper insight into these processes is also critical for the development of targeted immunomodulatory strategies for neuroinflammatory and neurodegenerative diseases. Here, we identify the lipid-binding immune receptor CD300f as a central regulator of microglial sensing and response to tissue damage and apoptotic cells *in vivo*. CD300f is required not only for efficient efferocytosis but also for activating intracellular processing pathways necessary for apoptotic cell degradation, underscoring its importance in maintaining CNS homeostasis and promoting inflammation resolution.

Two functionally and mechanistically distinct forms of microglial motility have been described. Directed motility toward a laser-induced tissue lesion or a source of ATP is mediated by P2Y12 receptors (Haynes, 2006; Madry, 2018). Microglia from mice lacking P2Y12 receptors exhibit normal baseline motility but are unable to polarize, migrate, or extend processes toward a specific stimulus (Haynes, 2006). In contrast, microglial ramification and surveillance of the brain are fundamentally dependent on the tonic activity of THIK-1 channels and do not require P2Y12 activity (Madry, 2018). CD300f deficiency preserved baseline surveillance but markedly impaired directed motility toward focal laser injury, phenocopying defects reported in TREM2$^{-/-}$ mice (Mazaheri, 2017). This suggests a potential functional convergence between CD300f and lipid receptors in coordinating damage detection. The directed motility impairment may stem from impaired sensing or interpretation of local DAMP gradients, including purinergic cues such as ATP and UDP released at the injury site.

A limitation of our laser injury model is the inability to determine the identity of the lesioned cell type, which may contribute to the inter-animal variability in microglial responses observed between animals. Future studies should explore whether different injury contexts—such as vascular, neuronal, or astrocytic damage—elicit distinct DAMP profiles that differentially activate microglia. An additional limitation of our study is that heterozygous mice for CX3CR1 were used for the laser lesion experiments and for some of the *in vivo* apoptotic cell efferocytosis evaluations. This may have unexpected interactions with the absence of CD300f. However, several findings from the *in vivo* and *in vitro* efferocytosis experiments were independently confirmed using CD300f$^{-/-}$ mice alone.

During tissue injury, stressed neurons and damaged cells release purines such as ATP and UDP, which act as DAMPs, activating purinergic receptors on microglia, initiating calcium signaling (Koizumi, 2007). The mechanism underlying the impaired directed motility in CD300f$^{-/-}$ microglia is not clear. We did not observe significant changes in P2RY12 protein, and no alteration in P2RY12 or the THIK-1 (*Kcnk13)* mRNA was described *in vivo* in CD300f deficient microglia (Lago, 2020), suggesting that CD300f may modulate either P2RY12 activation directly or indirectly affect some of its downstream effects that mediate directed motility, rather than its expression levels. In fact, P2RY12 has been shown to be modulated by phosphorylation (Kamiyama, 2017). While ATP promotes process extension via P2RY12, UDP primarily signals through the microglial-specific P2RY6 receptor to drive phagocytosis and the morphological transition to an amoeboid state (Koizumi, 2007; Umpierre et al., 2024). In models of neurodegeneration and trauma, activation of P2RY6 enhances apoptotic cell clearance, whereas its inhibition prevents morphological transition leading to increased parenchymal dead cell accumulation. In line with this, CD300f$^{-/-}$ microglia exhibit defective process extension, impaired transition to phagocytic phenotype and reduced phagocytosis *in vivo*. We show that these defects are accompanied by reduced P2ry6 mRNA levels post-CCI, as well as a marked increase in ENTPD6 (CD39L2) protein levels—a UDP-degrading ectonucleotidase (Hicks-Berger et al., 2000)—at the lesion site. Together, these findings suggest that reduced P2RY6 expression in CD300f$^{-/-}$ microglia blunts UDP-induced morphological transition and calcium signaling (Puigdellívol, 2021), while ENTPD6 upregulation may further deplete extracellular UDP, compounding the signaling deficit.

The microglial P2RY6 receptor – activated by extracellular UDP released by stressed neurons – is upregulated in microglia during *in vivo* neuronal death and is required for microglial phagocytosis of neurons (Puigdellívol, 2021). Loss of P2RY6 not only strongly attenuates spontaneous microglial calcium signaling, but was associated with reduced pro-inflammatory cytokine production, deficits in microglial phagocytosis, and enhanced CA3 neuron survival after epileptogenesis (Umpierre et al., 2024). In accordance with our results, the inhibition of microglial P2RY6 prevented the transition from ramified to phagocytic microglia and increased the number of dead cells in the brain parenchyma in the same mTBI model used here (Roth, 2014). Mechanistically, CD300f binds phosphatidylserine on apoptotic cells, recruits PI3K, and activates Rac/Cdc42 to drive actin remodeling (Tian, 2014) —pathways necessary for transition to a phagocytic phenotype, and which appear impaired in its absence.

In line with this, P2ry6 deletion reduced microglial engulfment and spares stressed neurons, but at the cost of disrupted circuit homeostasis in models of epilepsy, β-amyloid injection and tauopathy (Puigdellívol, 2021). This paradox, tissue and neuronal preservation combined with impaired functional recovery, mirrors our findings in CD300f-deficient mice and underscores the importance of microglial resolution and remodeling, rather than neuroprotection alone, in driving meaningful recovery. Like TREM2, CD300f influence synaptic remodeling and neuroplasticity via phosphatidylserine binding-mediated synaptic pruning (Alí-Ruiz et al., 2023). Thus, CD300f may contribute not only to coordinating the clearance of damaged cells, but also to synaptic remodeling programs necessary for functional recovery, potentially contributing to persistent motor impairments despite histological preservation.

Proteomic profiling revealed broad alterations in CD300f$^{-/-}$ lesioned brain affecting pathways beyond purinergic sensing. Differential expression included autophagy machinery components (ATG101, AMBRA1, RUBCN, TANK), mitophagy regulators (MFN1, USP30, WIPI1), and enzymes involved in glycerophospholipid remodeling (PISD, PLD4, AGPAT4). Upregulation of lipid catabolism enzymes (LIPA, ABCD3, ACADVL) and glycogen metabolism proteins (GYS1, PHKA1, PGM2) suggests compensatory activation of clearance and metabolic pathways. These findings align with prior reports of impaired glycolytic flexibility, reduced mitochondrial respiration, and transcriptional downregulation of lipid metabolism genes (e.g., Abcd1, Abcg1, Cpt1) in CD300f$^{-/-}$ microglia under inflammatory conditions (Lago, 2020). We further demonstrate that the deficiency of CD300f in microglia *in vivo* post-TBI fail to efficiently degrade apoptotic material over time. These findings are consistent with our *in vitro* results using CD300f-deficient BMDMs incubated with apoptotic thymocytes.

Importantly, these functional and metabolic changes occurred in the absence of overt inflammation. Core cytokines (e.g., IL-1β, TNFα, IFNγ, IL-6) mRNA and canonical activation marker proteins (e.g., AIF1, CD11b, GFAP, NFKB1/2, STAT1/2/3) remained unchanged. In addition, we did not observe increased leukocyte recruitment to the dura in CD300f$^{-/-}$ mice, further supporting the notion that enhanced inflammation does not account for the observed phenotypes. Morphometric analyses 3 months post-CCI revealed a reduction in amoeboid microglia near the lesion, suggesting a failure to fully transition into a phagocytic state. Downregulation of phagocytic markers mRNA such as *Sirpb1a* and *F2rl1*, along with compensatory upregulation of *MERTK* and *ELMO1* proteins (both essential for efferocytosis (Scott, 2001; Park, 2007), supports the notion of impaired engagement of efferocytic programs in CD300f$^{-/-}$ microglia. This interpretation is further supported by the failure of CD300f-deficient microglia to adopt an amoeboid morphology early after injury, despite normal proximity to dying cells. Thus, while CD300f$^{-/-}$ microglia can localize to sites of cell death, they exhibit impaired clearance. The upregulation of *MERTK* observed in our proteomic dataset likely represents an insufficient compensatory mechanism in response to incomplete efferocytosis. Together, these findings reinforce the role of CD300f in enabling the full activation of phagocytic pathways necessary for tissue homeostasis and repair.

Following TBI, the primary mechanical injury triggers a secondary cascade involving neuroinflammation, cell death, and tissue remodeling (Simon, 2017). While neuroinflammation is often associated with poor outcomes, it can also play protective roles depending on timing and context (Jassam et al., 2017). Both DAMPs and PAMPs modulate immune responses through ITAM- and ITIM-containing receptors such as TREM2 and CD300 family members (Colonna, 2023; Borrego, 2013). These lipid-binding immune receptors recognize diverse endogenous ligands, including apoptotic membranes and myelin debris and coordinate the phenotype of microglia and other myeloid cells beyond classical

inflammatory pathways (Deczkowska, 2018). For instance, stimulation of BMDM with the PAMP LPS induced a stronger NLRP3 activation in the absence of CD300f (Frances Evans, 2023). Interestingly, a novel mechanism of NLRP3 function has been proposed, which involves immunometabolism and not IL1β production. NLRP3 knockout macrophages upregulate *Slc1a3* glutamate transporter that provides increased TCA cycle substrates to the mitochondria and in this way stimulates microglial metabolism. Interestingly, they reported that CD300f is one of the few upregulated proteins in this condition, again linking CD300f, immunometabolic regulation. The unchanged levels of many pro-inflammatory factors, including IL1β, after CCI observed here further points towards other neuroprotective mechanisms of CD300f not related to classical inflammatory mechanisms, such as immunometabolic regulation of microglia.

Among myeloid cells, CD300f is expressed by circulating monocytes and neutrophils, which serve as early responders to injury in both peripheral tissues and the CNS (Kolaczkowska and Kubes, 2013). In models of mild TBI, neutrophils have been shown to contribute to apoptotic cell clearance and tissue repair within the dura, with minimal impact on the brain parenchyma (Roth, 2014). In contrast, our data suggest that in the context of mTBI, neutrophil participation in meningeal clearance is limited. We observed a reduction in neutrophil numbers without a corresponding change in PI^+ dead cell accumulation in the dura, suggesting that CD300f deficiency may compromise neutrophil recruitment or retention within these meningeal compartments. This effect may result from altered chemokine production by resident macrophages due to impaired detection of tissue damage in the absence of CD300f, and the expression of the classical neutrophil recruitment chemokine such Cxcl1 may be involved. Additionally, the absence of CD300f in myeloid cells did not alter permeability at the glial limitans superficialis, indicating that the observed parenchymal effects primarily reflect microglial, rather than peripheral, CD300f function. Together, these findings support a compartmentalized role for CD300f in orchestrating immune responses after TBI, with microglial CD300f being critical for apoptotic clearance and parenchymal remodeling.

In summary, CD300f orchestrates a multi-level microglial program encompassing DAMP sensing, purinergic signaling, efferocytosis, apoptotic cell metabolization and metabolic adaptation. The combined downregulation of P2ry6 and upregulation of ENTPD6 points to disrupted UDP signaling as a key defect impairing apoptotic cell recognition. These findings expand the functional relevance of CD300f to conditions beyond TBI, and contribute to the understanding of the broader mechanisms underlying pathologies in which this immune receptor has been involved including neuropsychiatric disorders (Lago, 2020; Kaufmann, 2021), autoimmunity (Tian, 2014; Tian, 2016), psoriasis (Danik, 2009), allergies (Izawa, 2012), aging (Frances Evans, 2023) and multiple sclerosis (Xi, 2010; Martínez-Barriocanal, 2017; Ban, 2010). Given that apoptotic cells elicit distinct cell states of phagocytes depending on context (Liebold, 2024), dissecting receptor-ligand interactions during the phagocytosis process remains critical. Just as TREM2 is being explored as a therapeutic target to enhance microglial repair (Wang, 2022; Colonna and Holtzman, 2025), future studies should investigate whether CD300f can be similarly targeted to modulate microglial responses and cells states and promote resolution and functional recovery in neuroinflammatory conditions.

4. Methods

4.1. Rodents

C57BL/6J (B6), B6.129P-Cx3cr1tm1Litt/J ($CX3CR1^{gfp/gfp}$) mice were obtained from The Jackson Laboratories. $CX3CR1^{gfp/+}$ reporter mice used in intravital two-photon microscopy were generated by crossing B6 mice with $CX3CR1^{gfp/gfp}$ mice and maintained in a closed breeding colony at the National Institutes of Health (NIH). B6.Cg-Cd300lftm1Jco/J ($CD300f^{-/-}$) mice were obtained from NIAID/NIH (Tian, 2014) and maintained at the NINDS facility under controlled environment. All mice were 8–16-week-old at the start of experiments and housed under specific pathogen-free (SPF) conditions in accordance with NIH Institutional Animal Care and Use Committee (IACUC) protocols.

For Controlled Cortical Injury (CCI) experiments, adult C57BL/6 (Charles River) WT mice and $CD300f^{-/-}$ (Genentech) were housed in the SPF facility of the Institut Pasteur de Montevideo (Uruguay) under a 12-hour light/dark cycle, with controlled temperature (20 ± 1 °C) and ad libitum access to food and water.

4.2. Intravital two-photon laser scanning microscopy and laser-induced injury

$CX3CR1^{gfp/+} \times CD300f^{-/-}$ or WT littermate mice of both sexes were used for live imaging of myeloid cells through the thinned-skull window at baseline and following mTBI. Imaging was performed using a Leica SP8 two-photon microscope equipped with a resonant scanner (8,000 Hz), a 25 × water-dipping objective (NA 1.0), quad HyD detectors, and a Mai Tai HP DeepSee laser (Spectra-Physics) tuned to 905 nm. For visualization of dead cells, PI (1 mg/mL; Thermo Fisher, #3P3566) was administered via transcranial incubation and intraperitoneal injection prior imaging. For vascular visualization, 100 µL of 1 mg/mL Evans blue (MilliporeSigma) in PBS was injected intravenously immediately before imaging. To label circulating neutrophils, mice received intravenous 488-conjugated anti-GR1 antibody (BD, #108406) five hours after mTBI and immediately prior to imaging. Artificial cerebrospinal fluid (aCSF; Harvard Apparatus, #597316) was applied to the skull surface to maintain immersion and image quality.

Laser injuries were induced by focusing the Mai Tai laser (100 % 1050 nm) for 2 min within a 17 µm ROI, followed by imaging at 905 nm. Z-stacks were captured at 1.0 µm (for laser injury) or 2.0 µm (for phagocytosis assays) intervals to depths of 20 and 70 µm, respectively. Time-lapse videos were acquired every 1 min for compression and every 22 s for laser ablation.

Quantification of microglial process extension into the lesion site was performed over 30 min using Imaris 9.6 image analysis software (Bitplane). A total of 10 and 12 lesions were analyzed from 6 wt and 6 CD300f−/− mice (5 males and 1 female per group; 8–12-week-old, except for one littermate pair aged 32 weeks). Each imaging session included at least one lesion per genotype, using littermate animals matched for age and sex. Two WT lesions showing atypical retraction responses and one $CD300f^{-/-}$ lesion showing excessive microglial activation were excluded. Despite consistent methodology, variable microglial responses were observed within each group, indicating additional sources of biological variability.

4.3. Skull thinning & compression injury

Mild TBI was induced as previously described (Manglani et al., 2018). 8–12-week-old mice were anesthetized with intraperitoneal injection of ketamine (85 mg/kg; Ketaset), xylazine (13 mg/kg; AnaSed), and acepromazine (2 mg/kg; VET One) in PBS. Body temperature was maintained at 37 °C. A scalp incision exposed the skull over the barrel cortex (2.5 mm lateral to bregma, 2.5 mm anterior to the sagittal suture), and a custom metal bracket was affixed to the skull. A 1 × 1 mm cranial window was thinned using a 0.5 mm dental drill to ~ 20–30 µm thickness over 1–2 min. Compression was applied by pressing a microsurgical blade vertically onto the thinned skull 10 times in rapid succession. This experiment was independently repeated 3 times, using a total of 14 wt mice (11 males and 3 females) and 12 $CD300f^{-/-}$ mice (8 males and 4 females).

4.4. Glial limitans leakage assay

To assess the integrity of the glia limitans superficialis, $CD300f^{-/-}$ or

WT mice were subjected to a mild compression injury and leakage assay was performed as described previously (Mason et al., 2021). Five hours after injury, 200 µL of sulforhodamine 101 (SR101, 1 mM; Sigma-Aldrich, S7635) in PBS was applied topically to the thinned skull for 12 min. The dye was then washed off with aCSF (Harvard Apparatus) over a 5-minute period. Three-dimensional Z-stacks were acquired using the two-photon microscope, starting just above the skull bone and extending 300 µm deep with a 1 µm step size. For quantification, Z-stacks were cropped to 250 µm to exclude skull autofluorescence. Mean fluorescence intensity (MFI) of SR101 signal (562–650 nm emission) was calculated using Imaris analysis software. This experiment was independently repeated 3 times using 8–12-week-old, age- and sex-matched littermate mice: 11 wt (9 males, 2 females) and 11 CD300f$^{-/-}$ (8 males, 3 females).

4.5. Controlled cortical impact (CCI)

Controlled cortical impact (CCI) was performed as described previously (Richter, 2018), using the PinPoint™ PCI3000 Precision Cortical Impactor (Hatteras Instruments). Adult WT and CD300f−/− mice (10–14-week-old) were anesthetized with isoflurane and secured in a stereotaxic frame. A midline incision exposed the skull, and a 3 mm craniotomy was created over the right cortex (between bregma and lambda, 0.5 mm lateral to the sagittal suture). The bone flap was removed. The impactor tip was centered over the right motor/somatosensory cortex (coordinates: L = 1.75 mm; AP = − 0.75 mm). A controlled impact was delivered with depth of 2 mm, velocity of 2 m/s, and dwell time of 150 ms. The experiment was conducted in two independent cohorts, each consisting of 6 male and 6 female littermate mice per genotype.

4.6. Behavior analysis

Sensorimotor deficits following CCI were assessed using the Parallel Rod Floor Test (Stoelting), with automated error and distance tracking via ANY-maze software, as described previously (Richter, 2018; Kamens and Crabbe, 2007).

Mice were tested pre-injury (baseline) and at multiple post-injury time points. Error frequency (errors per meter traveled) was normalized to the WT baseline average and expressed as fold change. Behavioral testing was performed during the light cycle under red-light illumination in a quiet environment. Video recordings were reviewed by a blinded experimenter to ensure scoring accuracy.

4.7. Histology and immunohistochemistry

Mice were perfused transcardially with 4 % paraformaldehyde (PFA), and brains were post-fixed in PFA for 2 h, then cryoprotected in 25 % sucrose for 48 h. Brains were embedded in OCT and frozen on dry ice. Coronal sections (30–100 µm) were obtained using a Leica CM1850 cryostat.

For immunostaining, free-floating brain sections and whole-mount meninges were blocked in 10 % FBS and 0.5 % Triton X-100 in PBS for 1 h at room temperature, followed by overnight incubation with primary antibodies in 1 % FBS and 0.5 % Triton X-100.

Brain slices: rabbit anti-Iba1 (1:700; Wako, #019-19741); goat anti-rabbit Alexa Fluor 488 (1:1000; Thermo Fisher, #A-11034); DAPI (1:500; Sigma-Aldrich, #D9542) for 10 min before mounting.

Dura whole-mounts: anti-Ly6G (1:200; BioLegend, #127626), anti-CD11b (1:200; BioLegend, #101220), and anti-laminin (1:200; Abcam, ab11575). After washing, the dura mater was carefully flattened on slides using a fine brush and mounted with FluorSave Reagent (MilliporeSigma). Slides were stored at 4 °C in the dark for 1 h before imaging. The laminin–lectin vascular repair assay was performed at 7 days post-TBI as previously described (Russo et al., 2018).

4.8. Confocal microscopy

Tile scans of brain sections and dura whole mount were acquired using an Olympus FV1200 laser-scanning confocal microscope with four detectors, six laser lines (405, 458, 488, 515, 559, 635 nm), and 4x, 10x, and 20 × objectives. Image analysis was performed using Imaris software.

4.9. Dead cell detection and quantification

To assess cell death in the parenchyma after compression injury, mice were incubated transcranially with propidium iodide (PI, 1 mg/mL; Thermo Fisher, #P3566) for 45 min, 4 h after mTBI.

In Fig. supplementary 2.c, PI$^+$ cells were quantified by generating surfaces in Imaris based on PI fluorescence intensity. Quantification was performed using five male mice per genotype.

In Fig. 3.c-d, analysis was conducted as described in (Mason et al., 2021). The section with the highest density of PI staining was imaged across the Z-axis. DAPI$^+$ surfaces were generated in Imaris, and PI$^+$ cells were defined as DAPI$^+$ nuclei co-localizing with PI signal. Counts were normalized within each experiment by calculating fold change relative to the average of WT animals. The experiment was conducted independently 3 times, with 11 wt and 8 CD300f$^{-/-}$ age- and sex-matched animals, respectively.

In Fig. 3a, microglial dynamics were tracked over a 30-minute period by intravital two-photon microscopy. The number of PI$^+$ cells showing ≥ 50 % volumetric overlap with microglia was recorded at two time points (2.5- and 3-hours post-injury). The phagocytosis rate was calculated as the proportion of newly engaged PI$^+$ cells between the two time points, normalized to the total number of PI$^+$ cells at 2.5 h. The experiment was conducted independently three times using three age- and sex-matched littermate mice per genotype.

4.10. Lesion quantification in CCI

For CCI: Parallel 30 µm coronal cryosections spaced 300 µm apart (every 11th section) were stained with cresyl violet (Nissl) following standard procedures (Peluffo, 2012). Tissue loss was quantified using Fiji software (NIH ImageJ), with side-by-side visual confirmation under 40 × magnification by two blinded observers. Slice "0″ was defined as the rostral coordinate where lateral ventricles first appear. The preserved area of the injured hemisphere was compared to the total area of the contralateral hemisphere. Data were expressed as percent tissue loss to account for potential edema.

Quantifications in the perilesional cortex by immunohistochemistry was performed as previously described (Henry, 2020). Sections were incubated in 10 % methanol + 2 % H_2O_2 in 30 % PBS to quench peroxidase activity, then blocked and incubated overnight at RT with rabbit anti-Iba1 (1:700; Wako) or anti-NeuN (Millipore #ABN78). Detection was performed using HRP-conjugated anti-rabbit IgG and DAB (0.5 mg/mL in PBS + H_2O_2). Neuronal and microglial counts and morphological classification (ramified, primed, ameboid), were performed in Fiji by a blinded investigator. Morphological criteria were based on prior literature and microglia was classified in: **Ramified**: thin processes > 650 µm, small soma (~10 µm^3), >20 branches**; Primed**: processes 300–550 µm, soma 50–75 µm^3, 20–30 branches and **Amoeboid**: thick processes ~ 200 µm, soma 80–100 µm^3, <10 branches. Data were expressed as percentage of total Iba1$^+$ cells per section. An average of five sections was analyzed per mouse.

4.11. Flow cytometry

Mild TBI was induced under aseptic conditions. At 24 h post-injury, 3–5 cortical punches (2 mm^2 each) were collected per genotype from age- and sex-matched animals, and pooled for downstream analysis. Tissues were dissociated using the Miltenyi Tumor Dissociation Kit

(#130-096-730) and GentleMACS Octo Dissociator with C Tubes (Miltenyi, #130-093-237). Myelin was removed with Myelin Removal Beads II (Miltenyi, #130-096-733), and $CD11b^+$ cells were enriched using anti-human CD11b MicroBeads (Miltenyi, #130-093-636). Cells were stained with LIVE/DEAD Fixable Blue viability dye (Thermo Fisher, #L34962) and a cocktail of surface antibodies for 20 min at room temperature. Microglia were identified as live, single cells positive for CD11b (BioLegend, #101237), CD45 (BioLegend, #103133), P2RY12 (BioLegend, #848006), and CX3CR1 (BioLegend, #149029). FMO and unstained controls were used for gating. Data acquisition was performed on a BD FACSymphony A5 and analyzed with FlowJo v10.9.0. Three independent experimental replicates were performed using age- and sex-matched animals (8–12 weeks old).

4.12. Apoptotic thymocytes assays

Apoptotic thymocytes (AT) were prepared as previously described (Krasemann, 2017). Thymi were dissociated through a 70 μm strainer and incubated overnight with 0.1 μM dexamethasone to induce apoptosis. ATs were labeled with CMTPX dye (Thermo Fisher, #C34552) and stereotactically injected into the cortex of 8–12-week-old $CD300f^{-/-}$ and WT mice (50,000 cells in 2 μL). Phagocytosis was assessed 3 h later by flow cytometry or two-photon microscopy. The experiment was independently repeated 4 times using age- and sex-matched animals, with a total of 7 wt (3 females, 4 males) and 8 $CD300f^{-/-}$ (4 females, 4 males) mice.

In vitro assays were conducted with bone marrow-derived macrophages (BMDM) generated as previously described (Frances Evans, 2023). Bone marrow was flushed from femurs and tibiae, plated in complete DMEM/F12 medium with 20 ng/mL M−CSF (BioLegend, #576406), and cultured in 100 mm non-tissue culture bacteriological Petry dishes. On day 4, cells were plated in 96 well plates at a density of 80,000 or 100,000 cells/well). AT were stained with CFSE (Thermo Fisher, #C34554), added to BMDM cultures for 15 min and analyzed by flow cytometry. For the clearance assay, BMDMs were incubated with apoptotic thymocytes for 4 h, after which non-internalized apoptotic cells were removed by extensive washing with warm PBS. BMDMs were then maintained in fresh complete medium for an additional 16 h to allow for processing and degradation of internalized apoptotic material. BMDM were harvested for flow cytometry acquisition and data were analyzed using FlowJo software (BD Biosciences). Phagocytic BMDMs were identified as cells positive for internalized CFSE-labeled AT.

4.13. Gene expression analysis

At designated time points post-injury (1 day for CCI; 5 h for mTBI), mice were perfused with cold PBS, and brains were rapidly dissected. A small region encompassing the lesion and surrounding superficial cortex (and meninges for mTBI) was collected and placed in RPMI medium on ice. Tissue was mechanically homogenized using sterile zirconia/silica beads (Biospec) in a bead mill homogenizer. Lysates were centrifuged at 12,000×*g* for 10 min at 4 °C, and RNA was extracted from the pellet using the RNeasy Plus Micro Kit (Qiagen, #74034). RNA was reverse transcribed into cDNA using standard protocols. Quantitative PCR was performed using SYBR Green Master Mix (Applied Biosystems) and a CFX96 Real-Time PCR Detection System (Bio-Rad). For CCI samples, pathway-targeted PrimePCR™ plates (Bio-Rad) for inflammation and phagocytosis pathways were used following manufacturer instructions. Reactions included 10–20 ng of cDNA per well. Each plate included quality controls for genomic DNA contamination and RNA integrity. Relative gene expression was calculated using the ΔΔCt method, normalizing to housekeeping genes *Gapdh* and *Actin*, and analyzed using Bio-Rad Gene Study software.

4.14. Proteomics

Data Independent Acquisition (DIA) mass spectrometry (MS) (by BGI, https://www.bgi.com/global/service/mass-spec-services/label-free-dia-quantitation) was used to obtain quantitative protein expression data for 10 samples (male and female littermate mice, 5 wt and 5 $CD300f^{-/-}$) of CCI mouse brains. A 3 mm x 3 mm x 3 mm sample of the lesion area was extracted from cold PBS perfused animals. After protein extraction, 100 μg protein was added to a 10KDa ultrafiltration tube and centrifuged at 20 °C and 12,000g for 20 min until the protein solution was completely centrifuged to the bottom of the collection tube. Then, 100 μL of 0.5 M TEAB was added, centrifuged at 20 °C and 12,000g for 20 min, a step that was repeated 3 times. In a new collection tube trypsin was added according to the ratio of trypsin enzyme: protein amount = 1:20 and reacted at 37 °C for 4 h. Samples were centrifugated at 20 °C and 12.000g for 15 min, the peptide solution after enzymatic digestion was collected at the bottom of the tube, and 100 μL of 0.5 M TEAB was added to the ultrafiltration tube, and centrifuged at 20 °C and 12,000g for 15 min. The collected peptide fractions were freeze-dried.

The DIA analysis by nano-LC-MS/MS was performed by reconstitution of the dried peptide samples with mobile phase A (H_2O, 0.1 % FA), centrifuged at 20,000g for 10 min, and the supernatant injected. The separation was performed using VanquishNeo liquid phase from Thermo. The sample entered an EASY-Spray™ HPLC column (150 μm × 15 cm, Thermo, USA) and was separated at a flow rate of 2.5 μl/min using the following effective gradient: 0 ~ 4 min, mobile phase B (80 % ACN, 0.1 % FA) linearly increased from 4 % to 25 %; 4 ~ 5.8 min, mobile phase B linearly increased from 25 % to 35 %; 5.8 ~ 6.2 min, mobile phase B increased from 35 % to 99 %, and the flow rate increased to 3 μl/min; 6.2 ~ 6.9 min, 99 % mobile phase B. The end of the nanoliter liquid phase separation was directly connected to the mass spectrometer.

Detection of peptides separated by liquid phase were ionized by nanoESI source and then entered into the tandem mass spectrometer Astral (Thermo, USA) for DIA mass spectrometry mode detection. Main parameter settings: ion source voltage was set to 1.8 kV; primary mass spectrometry scanning range was 380–980 *m/z*; resolution was set to 240,000; maximum ion injection time (MIT) was 5 ms; 380 ~ 980 *m/z* was divided into 300 windows for continuous window fragmentation and signal acquisition. The ion fragmentation mode was HCD, the fragmentation energy was set to NCE 25, the maximum ion injection time (MIT) was 3 ms, and the fragment ions were detected in Astral. AGC was set to: primary 500 %, secondary 500 %. After extracting ions peak area from the spectra produced in this experiment, the MSstats (Bioconductor) software package was used to finish system error correction and normalization for each sample. Final identification of proteins was obtained using Uniprot database.

A total of 119,302 peptides and 7366 proteins were identified (more than 6800 proteins per sample in all samples). The quality of the DIA data was evaluated based on intra-group coefficient of variation (CV), principal component analysis (PCA), and quantitative correlation of samples. Quantitative differential analysis was based on the quantitative values obtained for each protein in multiple replicates of the sample. This process used Welch's *t*-test to test the preset comparison group and calculate the multiple of differences. Two filtration criteria were used to get significant differential proteins: Fold change > 1.3 and Pvalue < 0.05). Pathway-based analysis was performed using Kyoto Encyclopedia of Genes and Genomes (KEGG) and Dr.Tom (BGI https://www.bgi.com/global/service/dr-tom) web application.

4.15. Statistical analysis

Statistical tests were selected based on data distribution and experimental design. Two-tailed unpaired Student's *t*-test was used for two-group comparisons for samples with equal variances or Welch's correction was applied for data with F test p value < 0.05. For multi-group comparisons, one-way ANOVA followed by Tukey's post hoc

test was applied. For repeated-measures data (e.g., behavior over time), two-way ANOVA with Sidak's post hoc test was used.

Significance was set at $P \leq 0.05$. All analyses were performed using GraphPad Prism version 10.0 (GraphPad Software, San Diego, CA).

Author contributions and acknowledgments

H.P. and L.N.D conceived the study. L.N.D performed most of the experiments. F.E., F.A.C., H.D.M Z.F D.A. N.L and R.LV. performed experiments. L.N.D. F.E. Z.F., and H.P. analyzed and discussed results. H.P. drafted the original manuscript and L.N.D and Z.F. contributed to the edition of the final version. All authors have read and agreed to the published version of the manuscript. We thank the staff of the URBE, Facultad de Medicina UDELAR (Uruguay), and Laboratory Animals Biotechnology Unit (UBAL), Advanced Bioimaging Unit (UBA) and Cell Biology Unit of the Institut Pasteur de Montevideo (Uruguay).

CRediT authorship contribution statement

Luciana Negro-Demontel: Writing – review & editing, Visualization, Methodology, Investigation, Formal analysis, Data curation, Conceptualization. **Frances Evans:** Methodology, Investigation, Formal analysis, Data curation. **Andrés Cawen:** Investigation, Formal analysis, Data curation. **Zachary Fitzpatrick:** Writing – review & editing, Investigation, Formal analysis. **Hannah D. Mason:** Investigation, Formal analysis. **Daniela Alí:** Investigation, Formal analysis. **Rubèn López-Vales:** Methodology, Investigation. **Natalia Lago:** Methodology, Investigation. **Hugo Peluffo:** Writing – review & editing, Writing – original draft, Supervision, Project administration, Methodology, Investigation, Funding acquisition, Formal analysis, Data curation, Conceptualization.

Funding

This work has been supported by grants from Comisión Sectorial de Investigación Científica (CSIC-UDELAR I + D 2012 ID 54), Uruguay; PEDECIBA, Uruguay; FOCEM (MERCOSUR Structural Convergence Fund), COF 03/1111; Banco de Seguros del Estado (BSE), Uruguay; International Centre for Genetic Engineering and Biotechnology (ICGEB, CRP/URY19-01), Grant PID2021-123272OB- I00 funded by MICIU/AEI/https://doi.org/10.13039/501100011033 and by "ERDF A way of making Europe", and the Intramural program of the National Institute of Neurological Disorders & Stroke (NINDS).

Appendix A. Supplementary data

Supplementary data to this article can be found online at https://doi.org/10.1016/j.bbi.2025.106105.

Data availability

Data will be made available on request.

References

Alí-Ruiz, D., Vitureira, N., Peluffo, H., 2023. Microglial CD300f immune receptor contributes to the maintenance of neuron viability in vitro and after a penetrating brain injury. Sci. Rep. 13, 16796.
Alvarez-Errico, D., et al., 2004. IREM-1 is a novel inhibitory receptor expressed by myeloid cells. Eur. J. Immunol. 34, 3690–3701.
Alvarez-Errico, D., Sayos, J., Lopez-Botet, M., 2007. The IREM-1 (CD300f) inhibitory receptor associates with the p85alpha subunit of phosphoinositide 3-kinase. J. Immunol. 178, 808–816.
Ban, M., et al., 2010. A non-synonymous SNP within membrane metalloendopeptidase-like 1 (MMEL1) is associated with multiple sclerosis. Genes Immun. 11, 660–664.
Borrego, F., 2013. The CD300 molecules: an emerging family of regulators of the immune system. Blood 121, 1951–1960.
Bosurgi, L. et al. Macrophage Function in Tissue Repair and Remodeling Requires IL-4 or IL-13 with Apoptotic Cells. https://www.science.org.
Choi, S.C., et al., 2011. Cutting edge: mouse CD300f (CMRF-35-like molecule-1) recognizes outer membrane-exposed phosphatidylserine and can promote phagocytosis. J. Immunol. 187, 3483–3487.
Cignarella, F., et al., 2020. TREM2 activation on microglia promotes myelin debris clearance and remyelination in a model of multiple sclerosis. Acta Neuropathol. 140, 513–534.
Colonna, M., 2023. The biology of TREM receptors. Nat. Rev. Immunol. https://doi.org/10.1038/s41577-023-00837-1.
Colonna, M., Holtzman, D.M., 2025. Rethinking TREM2 as a target for Alzheimer's disease after the INVOKE-2 trial failure. Preprint at Nat. Med.. https://doi.org/10.1038/s41591-025-03816-2.
Danik, J.S., et al., 2009. Novel loci, including those related to Crohn disease, psoriasis, and inflammation, identified in a genome-wide association study of fibrinogen in 17 686 women: the Women's Genome Health Study. Circ. Cardiovasc. Genet. 2, 134–141.
Davalos, D., et al., 2005. ATP mediates rapid microglial response to local brain injury in vivo. Nat. Neurosci. 8, 752–758.
De Schepper, S., Crowley, G., Hong, S., 2021. Understanding microglial diversity and implications for neuronal function in health and disease. Preprint at Dev. Neurobiol. 81, 507–523. https://doi.org/10.1002/dneu.22777.
Deczkowska, A., et al., 2018. Disease-associated microglia: a universal immune sensor of neurodegeneration. Preprint at Cell 173 (1073–1081). https://doi.org/10.1016/j.cell.2018.05.003.
Fourgeaud, L., et al., 2016. TAM receptors regulate multiple features of microglial physiology. Nature 532, 240–244.
Frances Evans, A., et al., 2023. CD300f immune receptor contributes to healthy aging by regulating inflammaging, metabolism, and cognitive decline. Cell Rep.. 42, 113269.
Gaikwad, S., et al., 2009. Signal regulatory protein-β1: a microglial modulator of phagocytosis in Alzheimer's disease. Am. J. Pathol. 175, 2528–2539.
Haynes, S.E., et al., 2006. The P2Y12 receptor regulates microglial activation by extracellular nucleotides. Nat. Neurosci. 9, 1512–1519.
Henry, R.J., et al., 2019. Microglial depletion with CSF1R inhibitor during chronic phase of experimental traumatic brain injury reduces neurodegeneration and neurological deficits. bioRxiv 40, 2960–2974.
Henry, R.J., et al., 2020. Microglial depletion with CSF1R inhibitor during chronic phase of experimental traumatic brain injury reduces neurodegeneration and neurological deficits. J. Neurosci. 40, 2960–2974.
Hickman, S.E., et al., 2013. The microglial sensome revealed by direct RNA sequencing. Nat. Neurosci. 1–12. https://doi.org/10.1038/nn.3554.
Hicks-Berger, C.A., Chadwick, B.P., Frischauf, A.M., Kirley, T.L., 2000. Expression and characterization of soluble and membrane-bound human nucleoside triphosphate diphosphohydrolase 6 (CD39L2). J. Biol. Chem. 275, 34041–34045.
Ising, C., et al., 2019. NLRP3 inflammasome activation drives tau pathology. Nature. https://doi.org/10.1038/s41586-019-1769-z.
Ivanenkov, V.V., Murphy-Piedmonte, D.M., Kirley, T.L., 2003. Bacterial expression, characterization, and disulfide bond determination of soluble human NTPDase6 (CD39L2) nucleotidase: Implications for structure and function. Biochemistry 42, 11726–11735.
Izawa, K., et al., 2012. The receptor LMIR3 negatively regulates mast cell activation and allergic responses by binding to extracellular ceramide. Immunity 37, 827–839.
Jaffa, A.A., et al., 2021. Modulation of neuro-inflammatory signals in microglia by plasma prekallikrein and neuronal cell debris. Front. Pharmacol. 12.
Jassam, Y.N., Izzy, S., Whalen, M., McGavern, D.B., El Khoury, J., 2017. Neuroimmunology of traumatic brain injury: time for a paradigm shift. Neuron 95, 1246–1265.
Kamens, H.M., Crabbe, J.C., 2007. The parallel rod floor test: a measure of ataxia in mice. Nat. Protoc. 2, 277–281.
Kamiyama, M., et al., 2017. ASK1 facilitates tumor metastasis through phosphorylation of an ADP receptor P2Y 12 in platelets. Cell Death Differ.. 24, 2066–2076.
Kaufmann, F.N., et al., 2021. Sex-dependent role of CD300f immune receptor in generalized anxiety disorder. Brain Behav.. Immun. Health 11, 100191.
Koizumi, S., et al., 2007. UDP acting at P2Y6 receptors is a mediator of microglial phagocytosis. Nature 446, 1091–1095.
Kolaczkowska, E., Kubes, P., 2013. Neutrophil recruitment and function in health and inflammation. Preprint at Nat. Rev. Immunol. 13, 159–175. https://doi.org/10.1038/nri3399.
Krasemann, S., et al., 2017. The TREM2-APOE pathway drives the transcriptional phenotype of dysfunctional microglia in neurodegenerative diseases article the TREM2-APOE pathway drives the transcriptional phenotype of dysfunctional microglia in neurodegenerative diseases. Immunity 47, 566-581.e9.
Lago, N., et al., 2020. CD300f immunoreceptor is associated with major depressive disorder and decreased microglial metabolic fitness. Proc. Natl. Acad. Sci. USA 117, 6651–6662.
Liebold, I., et al., 2024. Apoptotic cell identity induces distinct functional responses to IL-4 in efferocytic macrophages. Science (1979) 384.
Madry, C., et al., 2018. Microglial ramification, surveillance, and interleukin-1β release are regulated by the two-pore domain K+ channel THIK-1. Neuron 97, 299–312.e6.
Manglani, M., Gossa, S., McGavern, D.B., 2018. Leukocyte isolation from brain, spinal cord, and meninges for flow cytometric analysis. Curr. Protoc. Immunol. 121, e44.
Martínez-Barriocanal, Á., et al., 2017. Effect of specific mutations in Cd300 complexes formation; potential implication of Cd300f in multiple sclerosis. Sci. Rep. 7.
Mason, H.D., Johnson, A.M., Mihelson, N.A., Mastorakos, P., McGavern, D.B., 2021. Glia limitans superficialis oxidation and breakdown promote cortical cell death after repetitive head injury. JCI Insight 6.
Mazaheri, F., et al., 2017. TREM 2 deficiency impairs chemotaxis and microglial responses to neuronal injury. EMBO Rep. 18, 1186–1198.

McManus, R., et al., 2022. NLRP3-mediated glutaminolysis regulates microglia in alzheimer's disease. SSRN Electron. J. https://doi.org/10.2139/ssrn.4178538.
Moshkovits, I., et al., 2015. CD300f associates with IL-4 receptor $α$ and amplifies IL-4–induced immune cell responses. Proc. Nat. Acad. Sci. https://doi.org/10.1073/pnas.1507625112.
Nimmerjahn, A., Kirchhoff, F., Kerr, J.N.D., Helmchen, F., 2004. Sulforhodamine 101 as a specific marker of astroglia in the neocortex in vivo. Nat. Methods 1, 31–37.
Nimmerjahn, A., Kirchhoff, F., Helmchen, F., 2005. Resting microglial cells are highly dynamic surveillants of brain parenchyma in vivo. Science 1979 (308), 1314–1318.
Nugent, A.A., et al., 2020. TREM2 regulates microglial cholesterol metabolism upon chronic phagocytic challenge. Neuron 105, 837–854.e9.
Park, D., et al., 2007. BAI1 is an engulfment receptor for apoptotic cells upstream of the ELMO/Dock180/Rac module. Nature 450, 430–434.
Peluffo, H., et al., 2012. Overexpression of the immunoreceptor CD300F has a neuroprotective role in a model of acute brain injury. Brain Pathol.. 22.
Puigdellívol, M., et al., 2021. The microglial P2Y6 receptor mediates neuronal loss and memory deficits in neurodegeneration. Cell Rep. 37.
Richter, M., et al., 2018. Thy1-YFP-H mice and the parallel rod floor test to evaluate short- and long-term progression of traumatic brain injury. Curr. Protoc. Immunol. 2018.
Roth, T.L., et al., 2014. Transcranial amelioration of inflammation and cell death after brain injury. Nature 505, 223–228.
Roth, T.L., et al., 2014. Transcranial amelioration of inflammation and cell death after brain injury. Nature 505, 223–228.
Russo, M.V., Latour, L.L., McGavern, D.B., 2018. Distinct myeloid cell subsets promote meningeal remodeling and vascular repair after mild traumatic brain injury article. Nat. Immunol. 19, 442–452.
Scott, R.S., et al., 2001. Phagocytosis and clearance of apoptotic cells is mediated by MER. Nature 411, 207–211.
Simon, D.W., et al., 2017. The far-reaching scope of neuroinflammation after traumatic brain injury. Nature Publ. Group. https://doi.org/10.1038/nrneurol.2017.13.
Takahashi, K., Rochford, C.D., Neumann, H., 2005. Clearance of apoptotic neurons without inflammation by microglial triggering receptor expressed on myeloid cells-2. J. Exp. Med. 201, 647–657.
Tian, L., et al., 2014. P85alpha recruitment by the CD300f phosphatidylserine receptor mediates apoptotic cell clearance required for autoimmunity suppression. Nat. Commun. 5, 1–15.
Tian, L., et al., 2016. Enhanced efferocytosis by dendritic cells underlies memory T-cell expansion and susceptibility to autoimmune disease in CD300f-deficient mice. Cell Death Differ.. 23, 1086–1096.
Umpierre, A.D., Li, B., Ayasoufi, K., Johnson, A.J., Li, Y., 2024. Microglial P2Y 6 calcium signaling promotes phagocytosis and shapes neuroimmune responses in epileptogenesis. Neuron 1–19. https://doi.org/10.1016/j.neuron.2024.03.017.
Wahane, S., et al., 2021. Diversified transcriptional responses of myeloid and glial cells in spinal cord injury shaped by HDAC3 activity. Sci. Adv. 7. https://www.science.org.
Wang, P., et al., 2022. Precise gene delivery systems with detachable albumin shell remodeling dysfunctional microglia by TREM2 for treatment of Alzheimer's disease. Biomaterials 281.
Xi, H., et al., 2010. Negative regulation of autoimmune demyelination by the inhibitory receptor CLM-1. J. Experiment. Med. 207, 7–16.